Electronic Supplementary Information

Enhancing Light Absorption by Colloidal Metal Chalcogenide Quantum Dots via Chalcogenol(ate) Surface Ligands

Carlo Giansante

CNR NANOTEC, Istituto di Nanotecnologia, via Monteroni, 73100 Lecce, Italy

email: carlo.giansante@nanotec.cnr.it

Experimental Methods.

Materials.

All chemicals were of the highest purity available unless otherwise noted and were used as received. Lead oxide (PbO, 99.999%), Cadmium oxide (CdO, 99.5%), oleic acid (technical grade 90%), 1-octadecene (ODE, technical grade 90%), bis(trimethylsylil)sulfide (TMS, synthesis grade), p-methylbenzenethiol (ArSH, 98%), p-aminothiophenol (D-ArSH, 97%), p-(trifluoromethyl)thiophenol (A-ArSH, 97%), 2,6-dimethylthiophenol (SE-ArSH, 95%), 1-butanethiol (AlSH, 99%), benzyl mercaptane (BzSH, 99%), thiophenol (PhSH, 97%), benzeneselenol (PhSeH, 97%), phenol (PhOH), benzoic acid (PhCOOH), 3-methylbenzenethiol (95%) were purchased from Sigma-Aldrich. Tri-n-octylphosphine oxide (TOPO 99%), tri-n-octylphosphine (TOP, 97%), tri-n-butylphosphine (TBP, 99%), Sulfur (S, 99%), and Selenium (Se, 99,99%) were purchased from Strem Chemicals. Octadecylphosphonic acid (ODPA, 99%) was purchased from Polycarbon Industries. Triethylamine (Et_3N, $\geq$ 99.5%) was purchased from Fluka. All solvents were anhydrous and were used as received. Acetone (99.8%) was purchased from Merck. Acetonitrile (99.8%), dichloromethane (99.8%), hexane (95%), methanol (99.8%), tetrachloroethylene (99%), and toluene (99.8%) were purchased from Sigma-Aldrich.

Colloidal metal chalcogenide QD synthesis.

All QDs were synthesized in three-neck flasks connected to a standard Schlenk line setup under oxygen- and moisture-free conditions according to slightly modified, well-established recipes.

Colloidal CdS QDs.

In a typical synthesis yielding zinc-blende CdS QDs,[S1] 1 mmol of CdO (128 mg) was mixed with 3 mmol (850 mg) of oleic acid and 50 g of ODE. The mixture was vigorously stirred and deaerated through repeated cycles of vacuum application and purging with nitrogen at about 80 °C. Then, the mixture was heated to above 200 °C to allow dissolution of CdO until the solution became colorless and optically clear, indicating the formation of cadmium(II)-oleate complex(es). The solution was cooled at 80 °C and repeatedly subjected to vacuum in order to eventually remove water formed upon cadmium(II)-oleate complex formation. The solution was then heated again under

nitrogen flow and stabilized at 300°C. At this point 0.5 mmol of S precursor (0.016g of S in 10g of ODE, previously prepared under nitrogen atmosphere) was swiftly injected and CdS QDs were allowed to grow at 250 °C for about 10 minutes. The heating mantle was then removed and the reaction quenched by compressed air. After the synthesis, CdS QDs were transferred to a nitrogen-filled glove box. The QDs were repeatedly (three times, including the first step on crude product, are usually enough) precipitated using excess acetone (or methanol) and then redissolved in toluene, filtered through a 0.2 μm polytetrafluoroethylene membrane then stored at room temperature in a glove box for subsequent use as ~1 mM toluene solutions.

In a typical procedure yielding wurzite CdS QDs,[S2] TOPO (3.300g), ODPA (0.600g) and CdO (0.100g) were mixed in a three-neck flask, heated to ca. 90°C and repeatedly subjected to vacuum-nitrogen cycles. Under nitrogen atmosphere, the reaction mixture was then heated to above 300°C to dissolve the CdO until the solution turns optically clear and colorless. The heating mantle was removed to cool the flask to about 90 °C and again subjected to vacuum-nitrogen cycles. The temperature was then raised to 320°C and let stabilize then a mixture of TMS (0.170g) and TBP (3g) was swiftly injected. The nanocrystals were allowed to grow at 250°C to adjust their final diameter. The temperature was then quenched by compressed air. Afterwards, the QDs were precipitated with MeOH, washed by repeated re-dissolution in toluene and precipitation with the addition of MeOH, and finally kept in toluene.

Colloidal CdSe QDs.

In a typical synthesis yielding zinc-blende CdSe QDs,[S3] 0.3 mmol of CdO were mixed with 3 equivalents of oleic acid with 0.05 M concentration in ODE. The mixture was vigorously stirred and deaerated through repeated cycles of vacuum application and purging with nitrogen at about 80 °C. Then, the mixture was heated to above 200 °C to allow dissolution of CdO until the solution became colorless and optically clear, indicating the formation of cadmium(II)-oleate complex(es). The solution was cooled at 80 °C and repeatedly subjected to vacuum in order to eventually remove water formed upon cadmium(II)-oleate complex formation. The solution was then heated again under nitrogen flow and stabilized at 300°C. At this point 1 equivalent of Se powder dispersed, but not dissolved, in ODE was swiftly injected and CdSe QDs were allowed to grow at 260 °C. The heating mantle was then removed and the reaction quenched by compressed air. After the synthesis, CdSe QDs were transferred to a nitrogen-filled glove box. The QDs were repeatedly (three times, including the first step on crude product, are usually enough) precipitated using excess acetone (or methanol) and then redissolved in toluene, filtered through a 0.2 μm

polytetrafluoroethylene membrane then stored at room temperature in a glove box for subsequent use as ~1 mM toluene solutions.

In a typical procedure yielding wurzite CdSe QDs,[S2] TOPO (3.000g), ODPA (0.280g) and CdO (0.060g) were mixed in a three-neck flask, heated to ca. 90°C and repeatedly subjected to vacuum-nitrogen cycles. Under nitrogen atmosphere, the reaction mixture was heated to above 300°C to dissolve the CdO until the solution turns optically clear and colorless. The heating mantle was removed to cool the flask to about 90 °C and again subjected to vacuum-nitrogen cycles. The temperature was then raised to the required injection temperature (around 380 °C) and let stabilize. Swift injection of the Se:TOP solution (0.058g Se + 0.360g TOP) followed. The injection temperature and the reaction time were modified in order to synthesize CdSe dots of different sizes. The reaction was then quenched by compressed air. Afterwards, the nanocrystals were precipitated with methanol, washed by repeated re-dissolution in toluene and precipitation with the addition of methanol, and finally kept in toluene.

Colloidal PbS QDs.

In a typical synthesis yielding rock salt PbS QDs,[S4] 2 mmol of PbO (450 mg) and 6 mmol (1700 mg) of oleic acid were mixed in 10 g of ODE. The mixture was vigorously stirred and deaerated through repeated cycles of vacuum application and purging with nitrogen at about 80 °C. The mixture was then heated to above 100 °C to allow dissolution of PbO until the solution became colorless and optically transparent, suggesting the complete formation of lead(II)-oleate complex(es). The solution was cooled at 80 °C and repeatedly subjected to vacuum in the attempt of removing water eventually released upon lead(II)-oleate complex formation. The solution was then heated again under nitrogen flow and the temperature stabilized at 110°C. At this point, 1 mmol of sulfur precursor (bis(trimethylsilyl)sulfide; 210 μL) in 2 mL of octadecene was swiftly injected. The heating mantle was immediately removed and the resulting colloidal solution was allowed to cool to room temperature. After the synthesis, PbS QDs were transferred to a nitrogen-filled glove box. The QDs were precipitated using excess acetone (1:4 vol/vol), centrifuged at 4000 rpm and then redissolved in toluene. Two additional precipitation-redissolution cycles were performed by using methanol and toluene. An estimate of solvent volumes (about 4 mL of toluene to dissolve the QD pellet and 2 mL of methanol to precipitate the QDs) is crucial to obtain subtly purified QDs, although inherently empirical. The PbS QD size was varied by changing the amount of oleic acid (from two to sixteen equivalents) added to PbO, keeping constant its total concentration in the reaction flask; eventual dilution yields larger nanocrystals. Oleylamine (2 mmol) was added to the Pb-oleate precursor to obtain PbS QDs with diameters below

2.5 nm. Stock toluene solutions with concentration of ~ 1 mM were prepared and stored at room temperature in the glove box for subsequent use.

Replacing Ligand and QD Solution Proparation.

Replacing ligand solutions were prepared in glove box by diluting as received chalcogenols or by adding one equivalent of triethylamine to dichloromethane 10-50 mM solutions of the thiols shown in Scheme 1: according to reported pK_a (in water, 6.5 and 10.8 for ArSH,[S5] and $Et_3N{\cdot}H^+$,[S6] respectively), the equilibrium, though established in much less polar dichloromethane, shifts towards the formation of the ammonium thiolate ionic couple. A qualitative demonstration relies in the formation of needle crystals upon dichloromethane evaporation from solutions containing equimolar amounts of 3-methylbenzenethiol and triethylamine, which are both liquids at room temperature; empirically, thiol fetor is somehow reduced upon amine addition. Triethylamine was not added to AlSH that is much weaker acid than aromatic analogs (pK_a for AlSH is 11.5);[S5] indeed, it has been previously shown that titration of PbS QDs with AlSH leads to spectral changes that are negligibly affected by the presence of triethylamine.[S7]

Colloidal QD solutions were prepared in glove by diluting as-synthesized, purified batches to the concentration of 0.2 - 10 μM (depending on QD size), which was spectrophotometrically determined by using the Lambert-Beer law and well-established relationship between QD size and molar absorption coefficients of colloidal CdS,[S8] CdSe,[S9] and PbS QDs.[S10] Dichloromethane was used as solvent for Cd chalcogenide QDs and for PbS QDs of diameter below 3 nm, whereas tetrachloroethylene was used for larger PbS QDs to avoid solvent absorption in the NIR spectral region; no appreciable differences were observed by using these two solvents for PbS QDs with diameter of about 3 nm.[S7] This also supports the negligible role played by dielectric effects on the optical band gap of colloidal QDs.

Ligand Exchange Procedure.

Post-synthesis QD surface chemical modification was performed in a closed system (e.g., a vial or a quartz cuvette as for spectrophotometric titration experiments) by adding aliquots of solutions of the replacing ligands (as described above) to dichloromethane (or tetrachloroethylene) solutions of colloidal QDs. Closed systems account for sealed containers that guarantee no exchange of matter with the surroundings: it specifically refers to the precise control of QD concentration, which is instead hampered in ligand exchange procedures that imply filtering[S11] or phase transfer.[S12]

The ligand exchange process suddenly occurs upon replacing ligand addition to QD solutions: this can be evaluated by naked eyes as band gap reduction for small CdS QDs shifts the optical absorption in the visible spectral range, thus turning the solution from colorless to yellow,[S13] whereas small PbS QDs undergo concomitant broadband optical absorption enhancement that makes the solution significantly darker.[S14] The modified absorption spectra are constant with time and do not show any light scattering ascribable to aggregation, as demonstrated by the negligible extinction of the incident light at energies below the first excitonic peak.

To obtain ligand-exchanged colloidal QD dispersions without pristine oleate ligands, further purification was performed. To this end, p-methylbenzenethiolate-capped QDs were precipitated with excess hexane and methanol, then redispersed in chlorinated solvents.[S7,S15] The purification steps of p-methylbenzenethiolate-capped QDs involves quantitative precipitation with excess hexane, further supporting the efficient replacement of oleate ligands: indeed, hexane is a good solvent for as-synthesized QDs, while it is not for p-methylbenzenethiolate-capped QDs (less apolar solvents had to be used in order to dissolve such QDs, such as dichloromethane and/or o-dichlorobenzene).

Swift addition of high ligand loads without shaking QD solutions cause precipitation. Do ligand exchange slowly.

Chalcogenol ligands stink! Use under fume hood; pour remnant solutions into bleach to reduce stench by oxidation; leave glassware in a bleach bath before washing (or disposal).

Materials Characterization.

UV-Vis-NIR Absorption Spectroscopy.

The optical absorption spectra of colloidal QDs were measured in suprasil quartz cuvettes with 1 cm path length and were recorded with a Varian Cary 5000 UV-Vis-NIR spectrophotometer. The ligand-induced optical band-gap reduction reaches plateau at given ligand-to-QD molar ratios, beyond which the absorption spectrum does not appreciably change, suggesting that the QD surface is no longer accessible to extra added ligands and thus suggesting also quantitative ligand exchange (see Figure 2; this is valid for oleate-capped metal chalcogenide QDs, while plateau is not reached with phosphonate-capped metal chalcogenide QDs). [S7,S10,S13-S17]

Transimission Electron Microscopy (TEM).

TEM images were recorded with a Jeol Jem 1011 microscope operated at an accelerating voltage of 100 kV. Samples for analysis were prepared by dropping a QD solution onto carbon-coated Cu grids and then allowing the solvent to evaporate in a vapor controlled environment. QD diameters were determined by statistical analysis of TEM images of several hundreds of QDs with the ImageJ software. [S7,S10,S13-S17]

Nuclear Magnetic Resonance Spectroscopy (NMR).

NMR spectra were recorded with a Bruker AV400 spectrometer operating at 400 MHz on 0.1 mM solutions of ME QDs in $CDCl_3$ (δ = 7.26 ppm) at 293 K, in presence of ferrocene (δ = 4.17 ppm) as internal standard to determine oleate ligand content. The addition of thiolate ligands was performed in a vial to allow proper mixing with QDs. Upon ArS^- addition, the vinylene peak ($\delta \approx 5.3$ ppm) slightly shifts and shows fine structure indicative of oleate displacement; concomitantly, the resonances of protons in orto and meta positions of the ArS^- ligands ($\delta \approx 7.0$ and 7.2 ppm) appear, as shown in Figures S1-3.

Theoretical Calculations.

Thermodynamics of ligand binding at the QD surface (eqs. S1-5), dielectric and quantum confinement effects on QD first exciton energy (S6-S8 and S9-S14, respectively), and Maxwell Garnett effective medium theory applied to intrinsic absorption coefficients at energies far from the QD band gap (eqs. S15-18) were estimated by using Mathematica and Sigmaplot softwares.

TEM images and NMR spectra of the QDs.

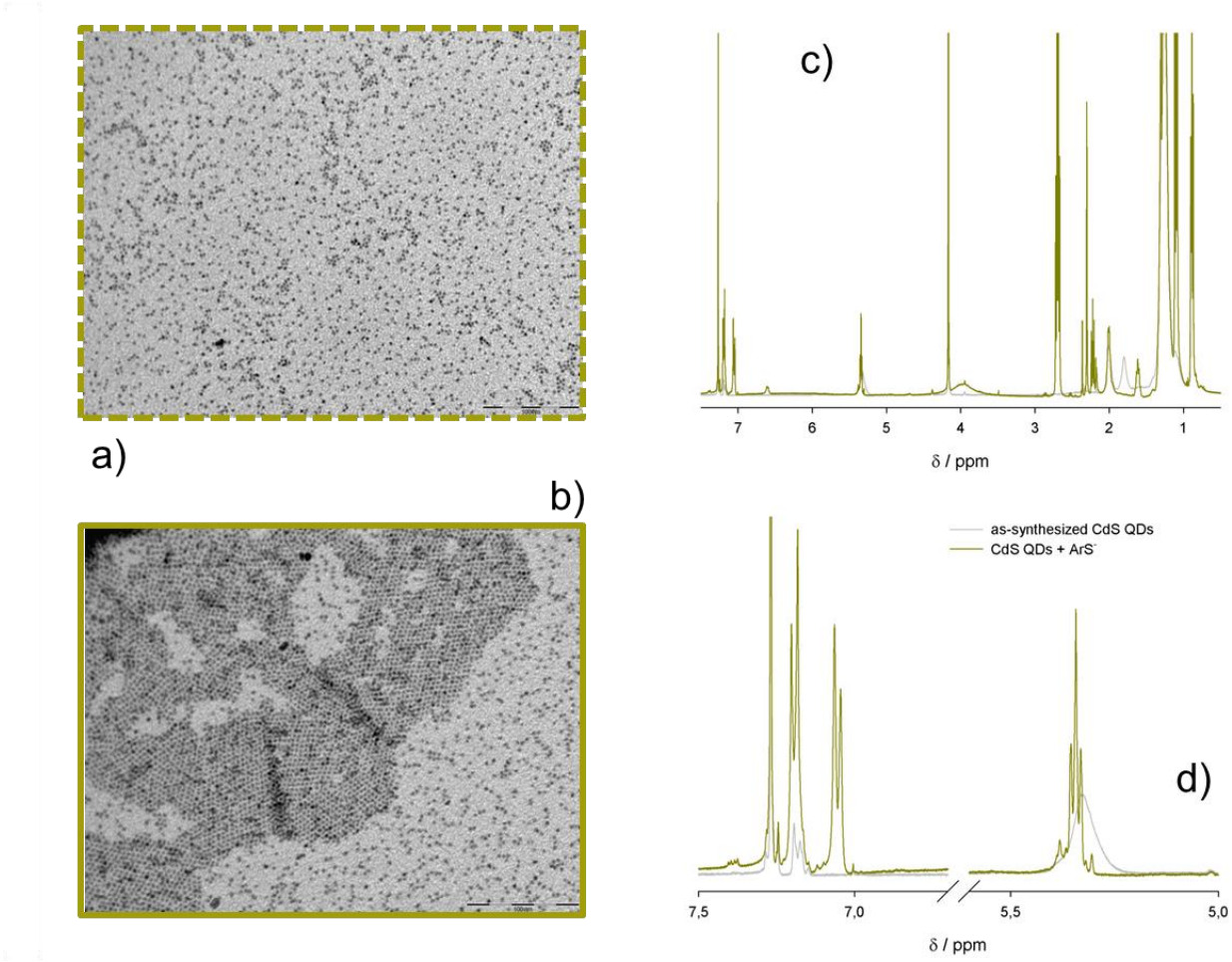

Figure S1. Transmission electron microscopy images of as-synthesized CdS QDs with diameter of about 2.8 nm (a) and upon addition of triethylammonium p-methylbenzenethiolate (b). NMR spectra (c) of as-synthesized CdS QDs (grey line) and upon addition of p-methylbenzenethiolate ligands (yellow line); panel (d) shows detail of the aromatic region.

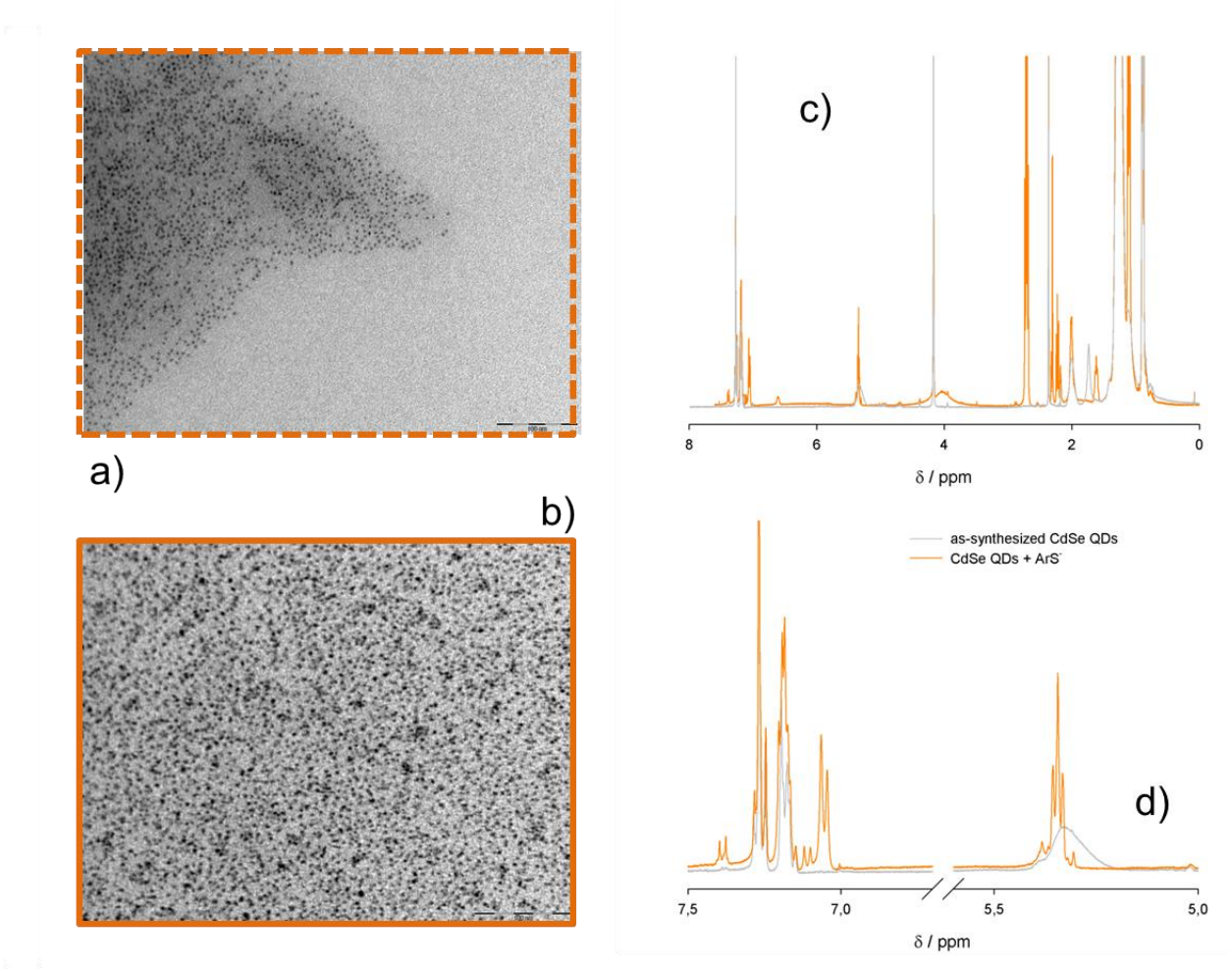

Figure S2. Transmission electron microscopy images of as-synthesized CdSe QDs with diameter of about 2.7 nm (a) and upon addition of triethylammonium p-methylbenzenethiolate (b). NMR spectra (c) of as-synthesized CdSe QDs (grey line) and upon addition of p-methylbenzenethiolate ligands (orange line); panel (d) shows detail of the aromatic region.

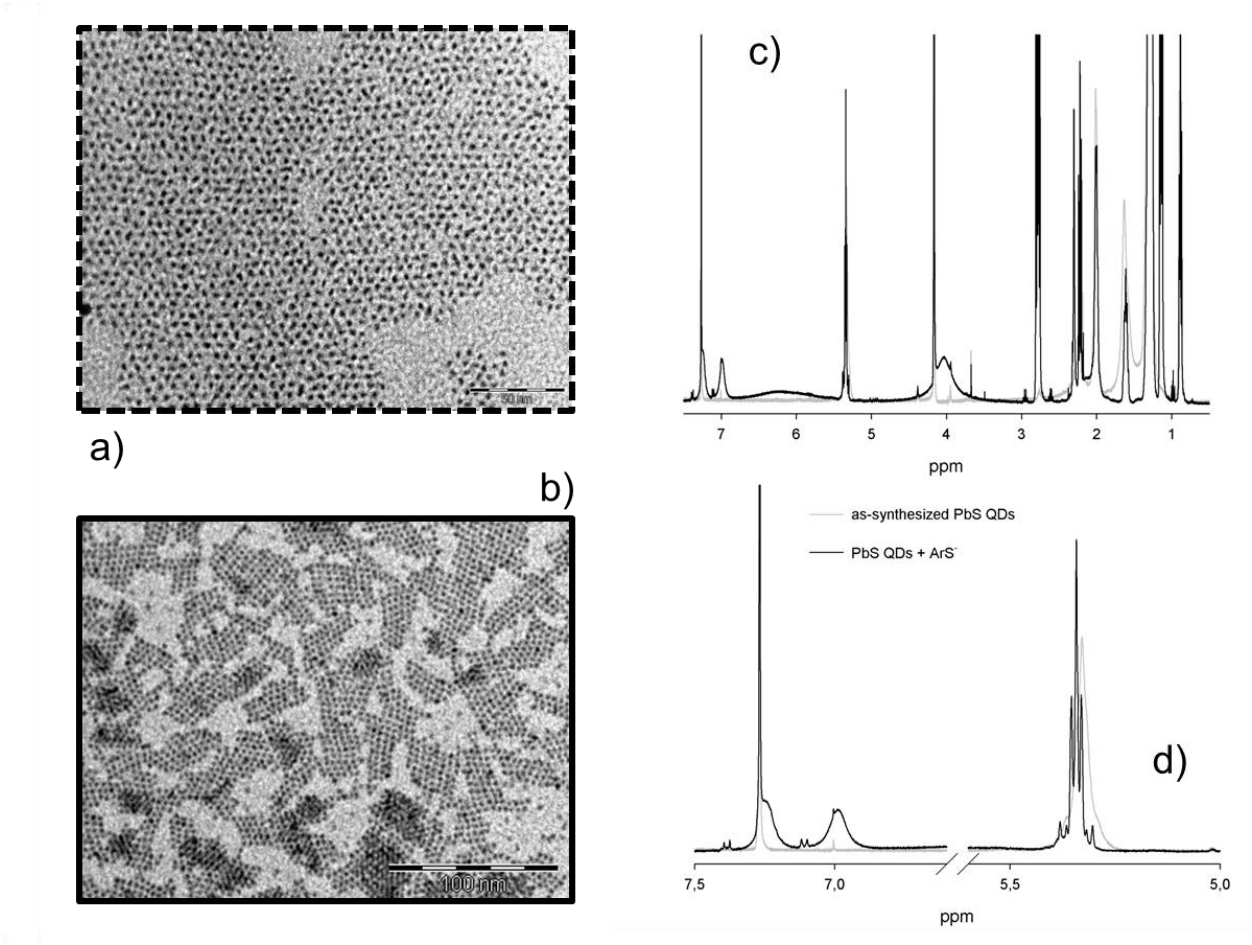

Figure S3. Transmission electron microscopy images of as-synthesized PbS QDs with diameter of about 2.9 nm (a) and upon addition of triethylammonium p-methylbenzenethiolate (b). NMR spectra (c) of as-synthesized PbS QDs (grey line) and upon addition of p-methylbenzenethiolate ligands (black line); panel (d) shows detail of the aromatic region.

Spectrophotometric titrations with p-methylbenzenethiolate of the QDs with cubic crystal lattice.

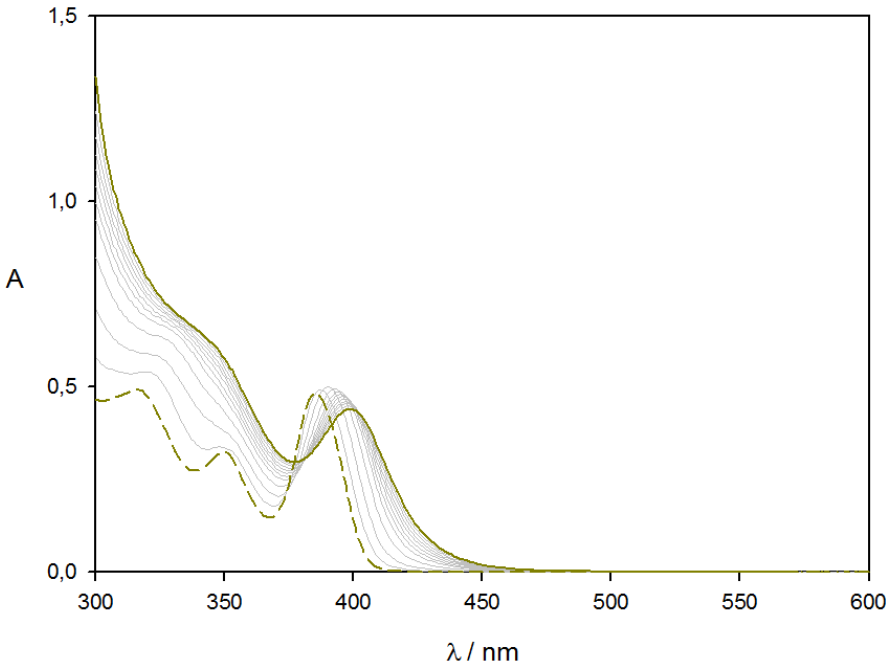

Figure S4. Optical absorption spectra of CdS QDs with diameter of about 2.8 nm upon titration with freshly prepared p-methylbenzenethiolate ligand solutions.

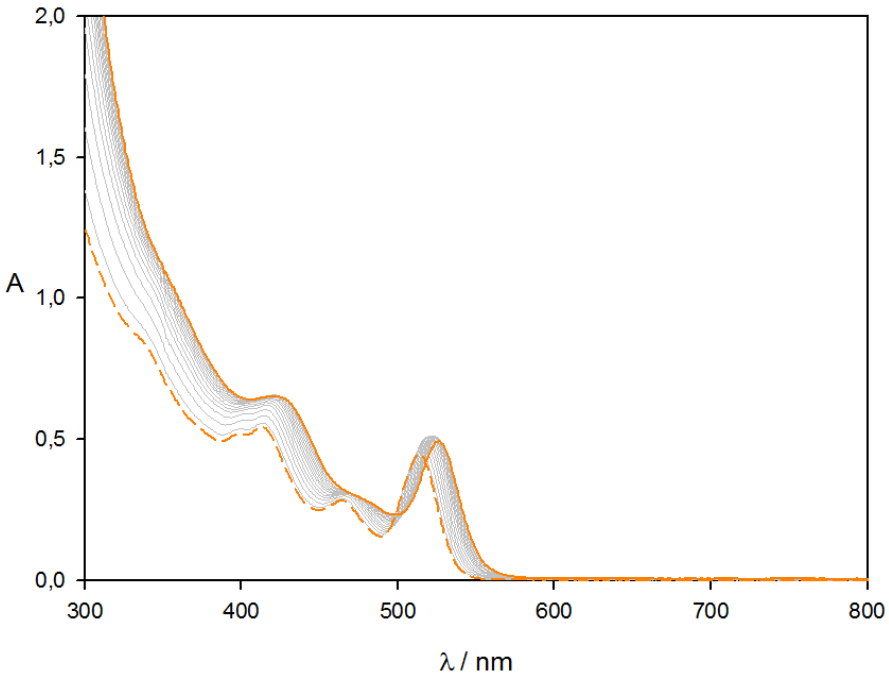

Figure S5. Optical absorption spectra of CdSe QDs with diameter of about 2.7 nm upon titration with freshly prepared p-methylbenzenethiolate ligand solutions.

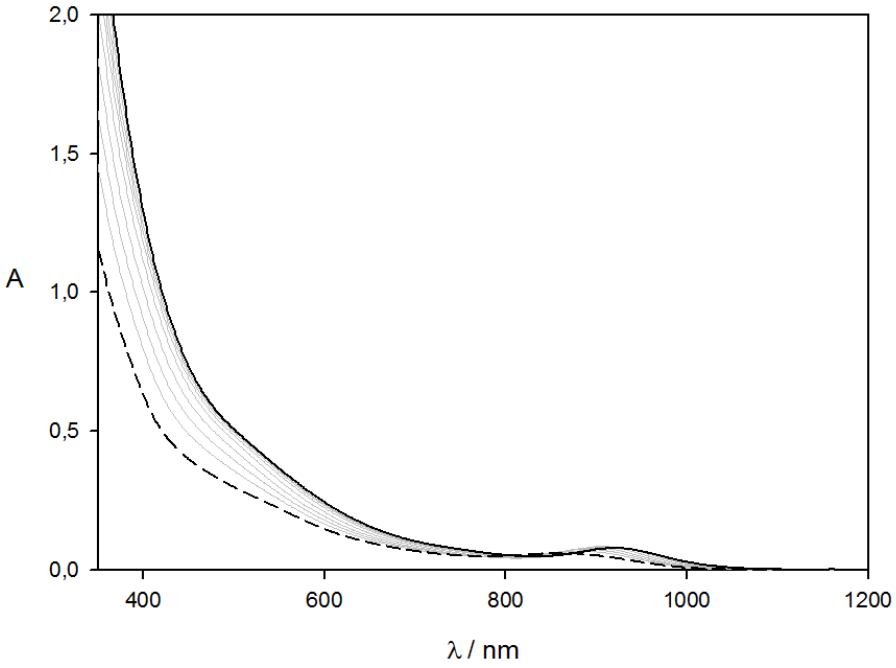

Figure S6. Optical absorption spectra of PbS QDs with diameter of about 2.9 nm upon titration with freshly prepared p-methylbenzenethiolate ligand solutions.

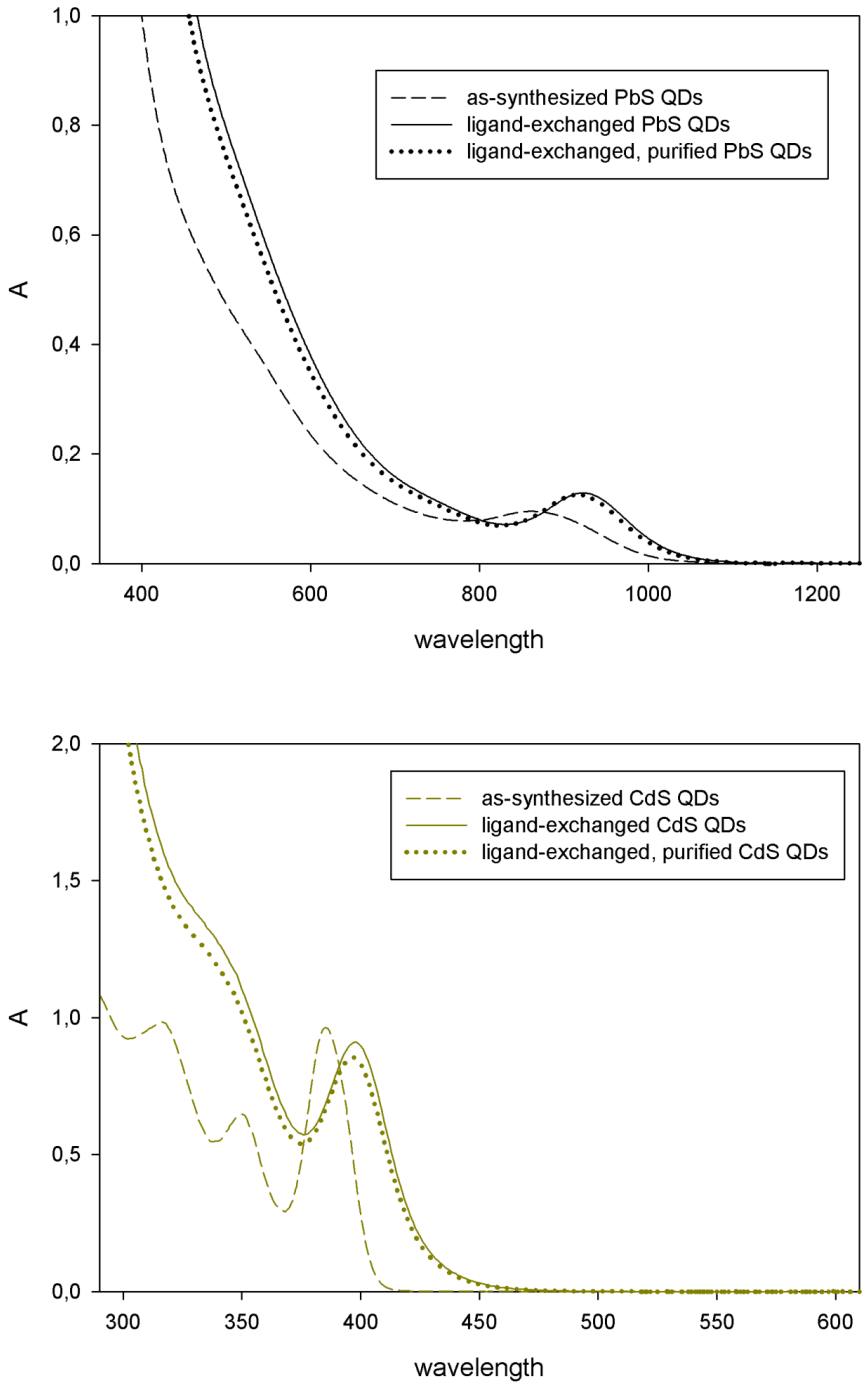

Figure S7. Optical absorption spectra of PbS (top) and CdS (bottom) QDs with diameter of about 2.9 nm ligand-exchanged with p-methylbenzenethiolate then purified by repeated precipitation in hexane/methanol and redispersion in chlorinated solvents, as previously reported.[S7,S15]

Ligand Binding Affinity Calculations.

Upon assuming that (*i*) the absorbance values recorded at wavelengths with expected bulk behavior are indicative of the extent of the ligand exchange process, (*ii*) the plateau indicates complete ligand exchange, (*iii*) the oleate displacement by thiolate ligands is thermodynamically highly favored, (*iv*) the number of binding sites per QD does coincide with the number of oleyl moieties, and (*iv*) the absence of cooperative binding, it is possible to estimate the association constants for each ArS^- ligand at the QD surface.

Given the equilibrium reaction between the as-synthesized ME QDs and the added ligands (ArS) leading to ME/ArS QDs:

$$ME + ArS \leftrightarrow ME/ArS \tag{S1}$$

the association constant of the reaction is

$$K_{ass} = \frac{[ME/ArS]_{eq}}{[ME]_{eq}[ArS]_{eq}} = \frac{[ME/ArS]_{eq}}{([ME]_0 - [ME/ArS]_{eq})([ArS]_0 - [ME/ArS]_{eq})} \tag{S2}$$

The observed absorbance at wavelengths sufficiently far from the band gap (λ) upon ArS^- addition, is related to the equilibrium concentration of the ME/ArS QDs formed in solution,

$$A_{obs}{}^{\lambda} = \varepsilon_{ME}{}^{\lambda}([ME]_0 - [ME/ArS]_{eq}) + \varepsilon_{ME/ArS}{}^{\lambda}([ME/ArS]_{eq}) + \varepsilon_{ArS}{}^{\lambda}([ArS]_0 - [ME/ArS]_{eq}) \tag{S3}$$

where $\varepsilon_{ME}{}^{\lambda}$ is as in references S8-10 and $\varepsilon_{ArS}{}^{\lambda} = 0$, thus the equilibrium concentration of the ME/ArS QDs can be derived by eq. S1:

$$[ME/ArS]_{eq} = \frac{1}{2K_{ass}}\left(a - \sqrt{a^2 - 4K_{ass}{}^2[ME]_0[ArS]_0}\right) \quad \text{(S4)}$$

where,

$$a = K_{ass}[ME]_0 + K_{ass}[ArS]_0 + 1 \quad \text{(S5)}$$

With this set of equations, it is possible to fit the experimental absorbance values as in Figure S7, which give the binding constant values reported in the main text (0.95×10^4 M^{-1} for CdS QDs, 0.72×10^4 M^{-1} for CdSe QDs, and 1.8×10^4 M^{-1} for PbS QDs).[S18]

The global association constant values can be obtained by multiplying for the number of oleyl ligands per QD as determined by quantitative NMR (i.e, about 110 for PbS QDs, and about 90 for CdE QDs).

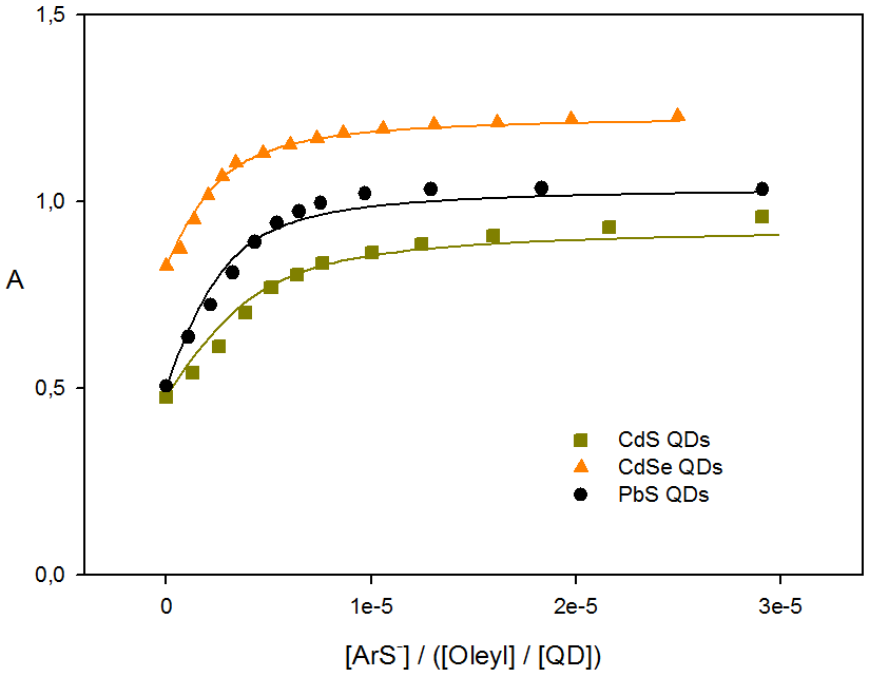

Figure S8. Plots of QD absorbance at wavelengths reported to correspond to bulk-like values, i.e. 310 nm for CdS, 340 nm for CdSe, and 400 nm for PbS, upon ArS^- addition; lines represent fitting according to supporting equations S1-5.

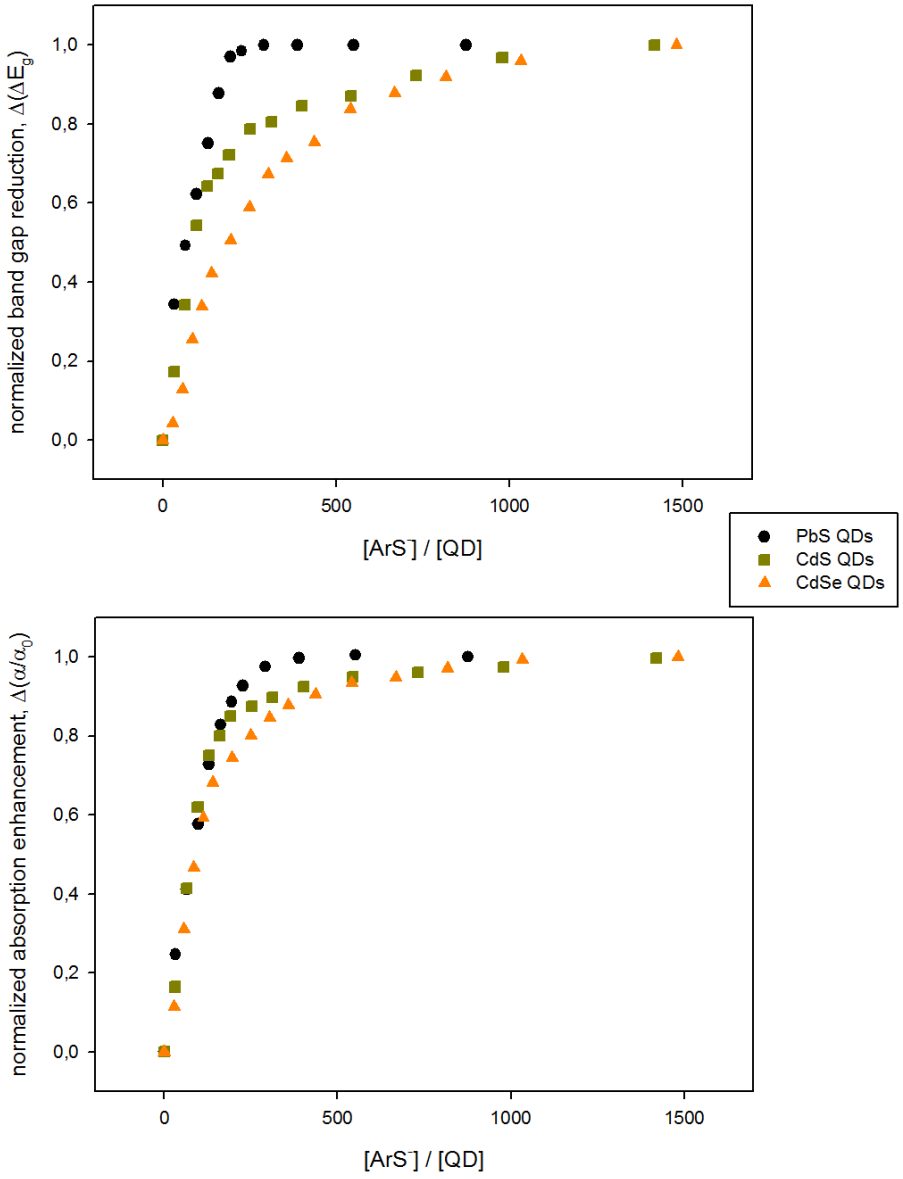

Figure S9. (top panel) Normalized plots of the ArS^--induced QD optical band gap reduciton (ΔE_g, as the difference between first exciton peak energy after and before ligand exchange). (bottom panel) Normalized plots of the ArS^--induced QD broadband optical absorption enhancement (α/α_0, as the ratio of energy integrated absorption coefficients after and before ligand exchange).

Spectrophotometric titrations with p-methylbenzenethiolate of the QDs with hexagonal crystal lattice.

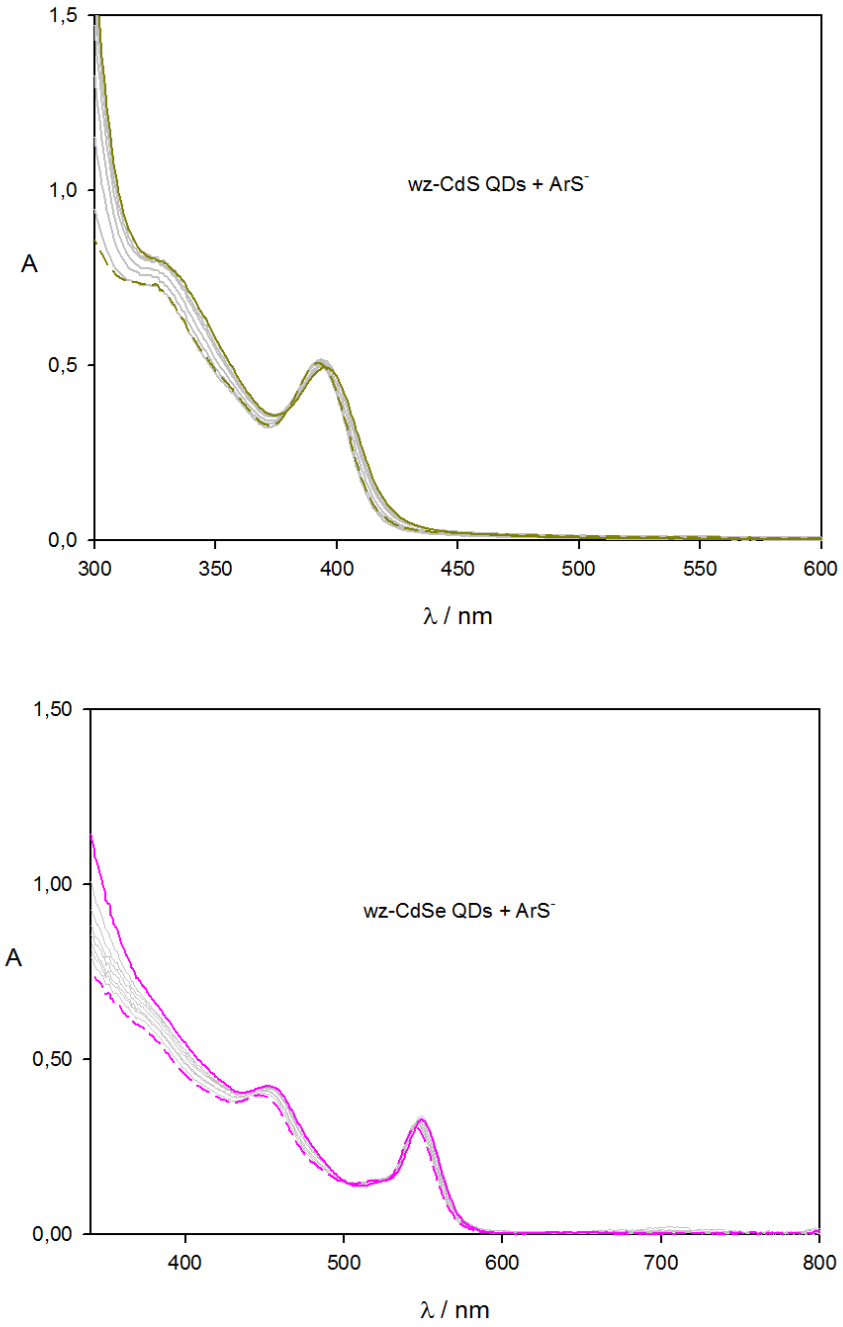

Figure S10. Absorbance spectra of wurzite (top panel) CdS and (bottom panel) CdSe QDs (dashed lines) upon addition of p-methylbenzenethiolate.

The role of the ligand binding atoms on the QD optical properties.

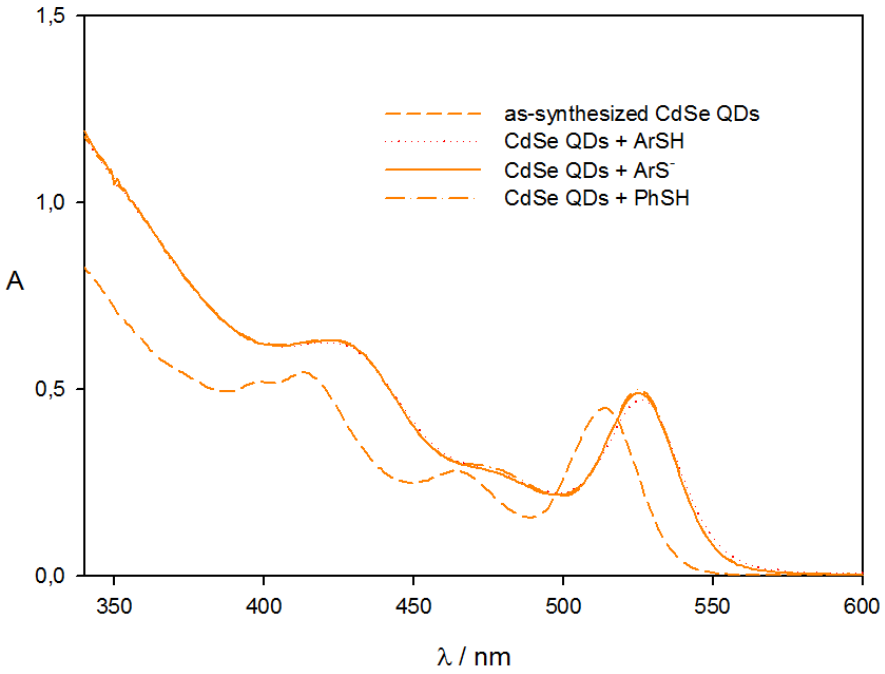

Figure S11. Absorbance spectra of zinc-blende CdSe QDs (dashed line) and upon addition of ArS^{-}, ArSH, and PhSH.

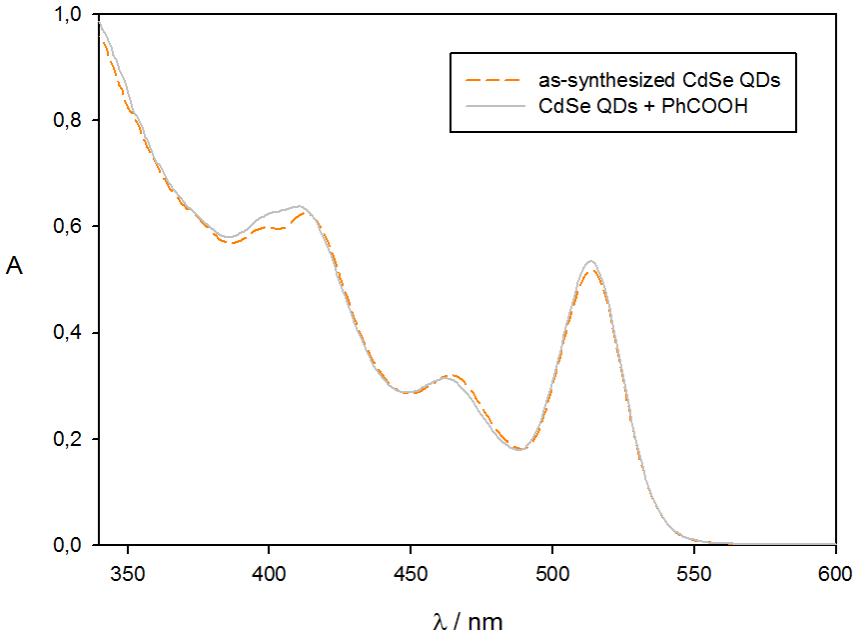

Figure S12. Absorbance spectra of zinc-blende CdSe QDs (dashed line) and upon addition of PhCOOH.

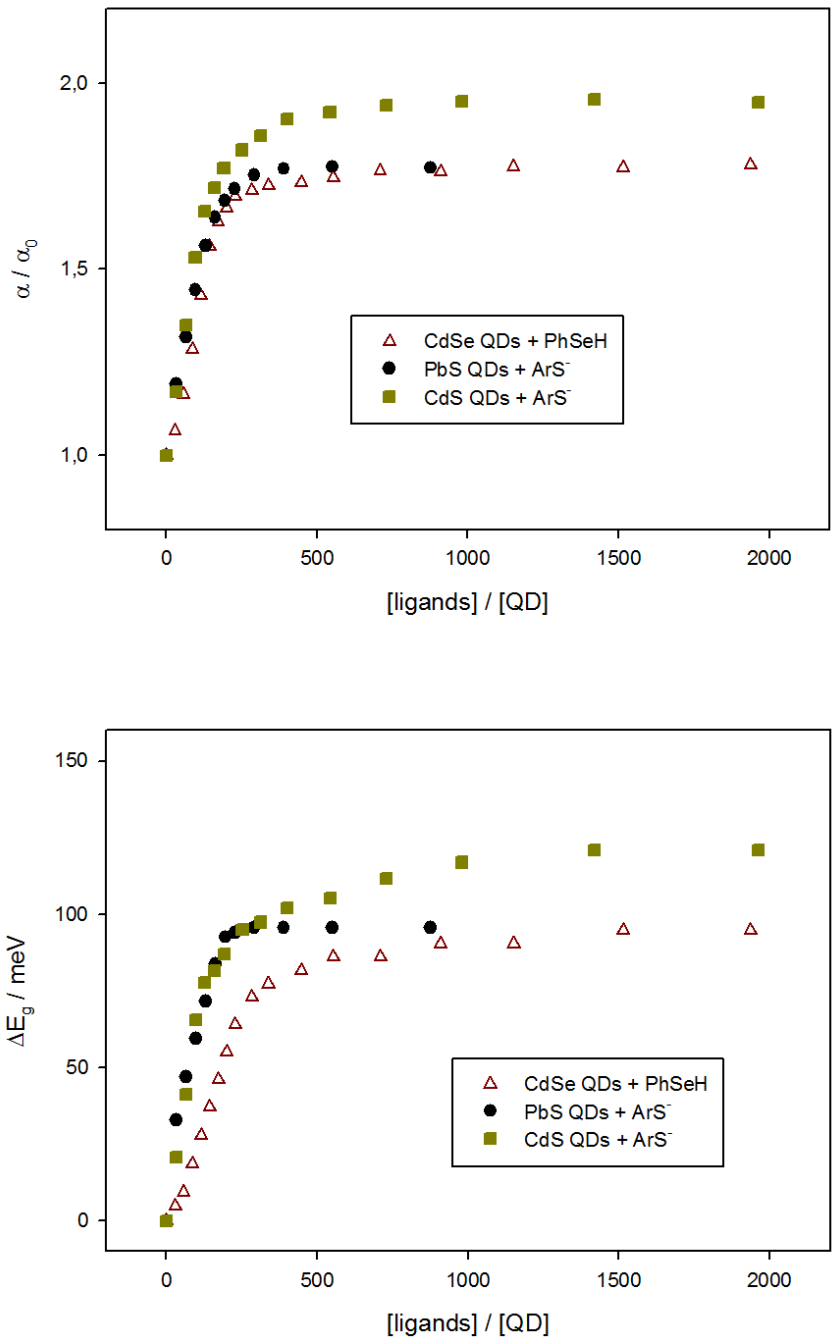

Figure S13. Plots of (top panel) broadband optical absorption enhancement and of (bottom panel) optical band gap reduction of CdS upon ArS^{-} addition, CdSe upon PhSeH addition, and PbS upon ArS^{-} addition.

Dielectric Confinement Effect Calculations.

The core/shell dielectric mismatch may induce surface polarization affecting exciton energy and was evaluated as follows. Upon using a two-state nearly free-electron model within the framework of effective mass approximation accounting for the energy of the first exciton transition in QDs, such polarization effect can be described under the assumption that bulk transport gap, kinetic energies of the electron and the hole due to quantum confinement, and the electron/hole electrostatic interaction are related only to the inorganic core and are therefore unaffected by ligand exchange; the observed bathochromic shift, ΔE_g, thus coincides with the difference in the polarization term upon ligand exchange, $\Delta\delta$, according to:[S19]

$$\Delta E_g \equiv \Delta\delta \tag{S6}$$

with,

$$\delta = \frac{\pi e^2}{\varepsilon_{QD}\varepsilon_0 d_{QD}} \sum_{l=1}^{\infty} \frac{d_{QD}}{2}^{2l+1} A_l \int_0^1 \left[j_0(\pi x)\right]^2 x^{2l+2} dx \tag{S7}$$

where ε_0 is the vacuum permittivity and ε_{QD} is high-frequency[S20] dielectric constant of the core constants (5.7 for CdS, for 10.2 CdSe, and 17.2 for PbS, as reported in the main text), d_{QD} is the QD diameter, e is the fundamental charge for the electron, $j_0(x)$ is the zero-order spherical Bessel function, and the term A_l is given by:

$$A_l = \frac{l+1}{\frac{d_{QD}}{2}^{2l+1}} \frac{\frac{d_{QD}}{2}^{2l+1} (\varepsilon_\ell - \varepsilon_s)[\varepsilon_c + l(\varepsilon_c + \varepsilon_\ell)] + \left(\frac{d_{QD}}{2} + L_\ell\right)^{2l+1} (\varepsilon_c - \varepsilon_\ell)[\varepsilon_s + l(\varepsilon_\ell + \varepsilon_s)]}{\frac{d_{QD}}{2}^{2l+1} (\varepsilon_c - \varepsilon_\ell)[(\varepsilon_{lig} - \varepsilon_{solv})l(l+1)] + \left(\frac{d_{QD}}{2} + L_\ell\right)^{2l+1} [\varepsilon_\ell + l(\varepsilon_c + \varepsilon_\ell)][\varepsilon_s + l(\varepsilon_\ell + \varepsilon_s)]} \tag{S8}$$

in which the dielectric constants for the ligand shell, ε_ℓ, are assumed as the square of the oleic acid and benzenethiol ligand refractive indexes (2.13 and 2.52, respectively), despite the severe approximation of attributing a dielectric constant to a sort of monolayer at the QD surface; the solvent high-frequency dielectric constant, ε_s, is taken as the square of the solvent refractive index (1.98);[S21] the ligand lengths, L_ℓ, are assumed as 1.8 nm for native oleate and 0.6 nm for replacing benzenethiolate. The optical band gap reduction expected from dielectric arguments is lower than a couple of meV for the size range here considered, as shown in Figure 6a and S13 (for PbS QDs).

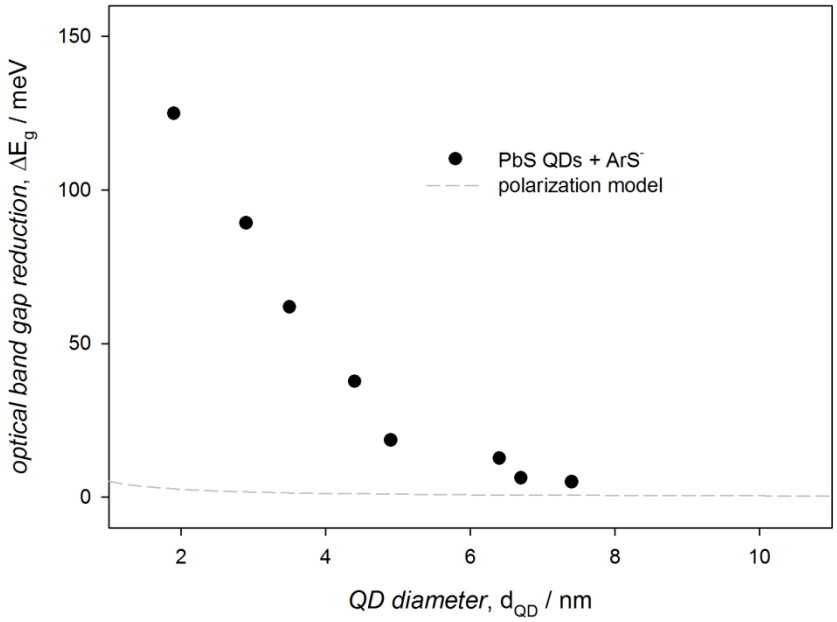

Figure S14. Plot of the first exciton peak red shift observed upon addition of ArS^- to solutions of colloidal PbS QDs. Dashed line is the polarization effect predicted according to equations S6-8 upon exchanging native oleate ligands for ArS^- on PbS QDs.

Quantum Confinement Effect Calculations.

The height of the potential barrier at the core interface with ligands may affect quantum confinement thus changing the QD first exciton energy and was evaluated as follows. Upon using a double spherical finite potential well model[S22,S23] within the framework of effective mass approximation accounting for the energy of the first exciton transition in QDs, the optical band gap reduction was related to the different kinetic energies of one of the charge carriers (the hole, presumably) under the assumption that bulk transport gap, kinetic energies of the other charge carrier (the electron, consequently) due to quantum confinement, and the electron/hole electrostatic interaction are unaffected by ligand exchange:

$$\Delta E_g \equiv \Delta E_h \tag{S9}$$

For the charge carrier under the action of a force:

$$\left[-\frac{\hbar^2}{2}\nabla\frac{1}{m}\nabla + V(\vec{r})\right]\psi(\vec{r}) = E_h\psi(\vec{r}) \tag{S10}$$

For a symmetric, stepwise potential:

$$V(\vec{r}) = V(r) = \begin{cases} V_c, & 0 \le r \le \dfrac{d_{QD}}{2} \\ V_\ell, & \dfrac{d_{QD}}{2} < r \le \dfrac{d_{QD}}{2} + L_\ell \\ V_s, & \dfrac{d_{QD}}{2} + L_\ell < r \end{cases} \tag{S11}$$

With $V_c = 0$, $V_\ell = 0$ and 2 eV for benzenethiolate and oleate, respectively, and $V_s = 5$ eV.

And the radial and spherical coordinates can be separated:

$$\psi(r,\theta,\phi)=\frac{1}{\sqrt{4\pi}}R(r) \tag{S12}$$

For the ground state (n = 1, l = m = 0).

$$R(r)=\begin{cases} A_c\, j(kr)+B_c n(kr), & 0\le r\le \dfrac{d_{QD}}{2} \\ A_\ell h^{(+)}(ikr)+B_\ell h^{(-)}(ikr), & \dfrac{d_{QD}}{2}<r\le \dfrac{d_{QD}}{2}+L_\ell \\ A_s h^{(+)}(ikr)+B_s h^{(-)}(ikr), & \dfrac{d_{QD}}{2}+L_\ell < r \end{cases} \tag{S13}$$

With *j, n, h* denote spherical Bessel, Neumann, and Hankel functions, respectively, and

$$k=\sqrt{\frac{2m|E_h-V|}{\hbar^2}} \tag{S14}$$

In the core, ligand, solvent regions, in which potential barrier height is defined above and m are the effective masses assumed as m_e for both ligand and solvent regions.

The solution must be continuous and derivable, regular for r = 0 and vanish at infinity, thus yielding a system of four linear equations for the four coefficients with non-trivial solutions if its determinant is 0; normalization permits to determine such coefficient values.

The optical band gap reduction expected from exciton delocalization for QDs with 3.0 nm diameter bearing oleate and benzenethiolate ligands is shown in Figures 6b and S14 (for PbS QDs).

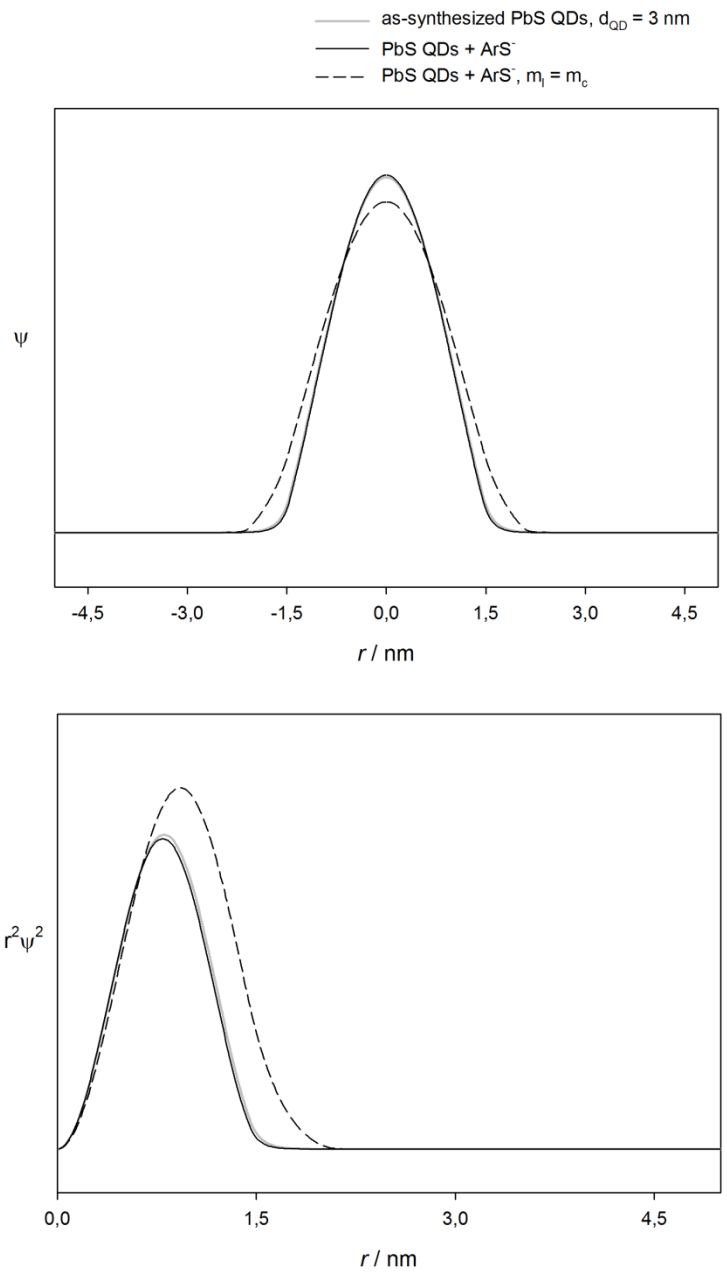

Figure S15. (top) wavefunctions in a 3.0 nm diameter PbS QD with oleate ligands (V_l = 2 eV, grey solid line), with benzenethiolate ligands (V_l = 0 eV, black solid line); and with benzenethiolate ligands ($m_l = m_c$ = 0.085, black dashed line). (bottom) radial wavefunction distribution as in the top panel.

Maxwell Garnett Effective Medium Theory Calculations.

The experimentally observed optical absorption enhancement induced by surface ligands highlights the limitations of formalisms mutuated from classic electromagnetism in describing the linear optical absorption of colloidal semiconductor nanocrystals. Indeed, the optical absorption of dilute dispersions of small colloidal crystals (where dilute stands for non-interacting particles –the volume fraction is much lower than one– and small indicates that the particles are much smaller than the wavelength of the incident light) surrounded by a dielectric medium (with much lower refractive index than the particle itself) is commonly described using formalisms derived from Maxwell Garnett effective medium theory.[S24] In this framework, the nanocrystal intrinsic absorption coefficient at energies sufficiently far from the band gap, under the assumption of a continuum density of states and in absence of intense transitions, matches, up to a multiplicative constant, the bulk value rescaled for the dielectric confinement as:

$$\mu_\lambda \propto \alpha_\lambda \left| f_{LF} \right|^2 \tag{S15}$$

where α_λ is the thickness-independent absorption coefficient of homogeneous, bulk ME and f_{LF} represents the Lorentz local field factor that relates the external, applied electric field and the electric field within the QD, accounting for the dielectric effect of the surroundings (the ligand shell and the solvent) on as-synthesized ME QDs, $f_{LF}{}^0$, and on ligand-exchanged ME QDs, f_{LF} . Such factor can be used to evaluate the intrinsic absorption coefficients at wavelengths with expected bulk behavior with an expression derived for core/shell QDs,[S25] albeit the severe approximation of assuming a dielectric constant for a sort of organic ligand monolayer at the inorganic core surface:

$$\left| f_{LF} \right|^2 = \left| \frac{9\varepsilon_{lig}\varepsilon_{solv}}{a\varepsilon_{lig} + 2b\varepsilon_{solv}} \right|^2 \tag{S16}$$

with,

$$a = \varepsilon_{core}\left(3 - 2\frac{\left(L_{lig} + \frac{d_{QD}}{2}\right)^3 - \left(\frac{d_{QD}}{2}\right)^3}{\left(L_{lig} + \frac{d_{QD}}{2}\right)^3}\right) + 2\varepsilon_{lig}\frac{\left(L_{lig} + \frac{d_{QD}}{2}\right)^3 - \left(\frac{d_{QD}}{2}\right)^3}{\left(L_{lig} + \frac{d_{QD}}{2}\right)^3} \quad \text{(S17)}$$

$$b = \varepsilon_{core}\frac{\left(L_{lig} + \frac{d_{QD}}{2}\right)^3 - \left(\frac{d_{QD}}{2}\right)^3}{\left(L_{lig} + \frac{d_{QD}}{2}\right)^3} + \varepsilon_{lig}\left(3 - \frac{\left(L_{lig} + \frac{d_{QD}}{2}\right)^3 - \left(\frac{d_{QD}}{2}\right)^3}{\left(L_{lig} + \frac{d_{QD}}{2}\right)^3}\right) \quad \text{(S18)}$$

where the high-frequency dielectric constant value is assumed as the dielectric constant for the ME core, ε_{core}; the square of the oleate and p-methylbenzenethiolate ligand refractive indexes and of dichloromethane (tetrachloroethylene) are assumed as the dielectric constants for the ligand shell and the solvent, ε_{lig} and ε_{solv}, respectively; 1.8 nm for oleate and 0.6 nm for p-methylbenzenethiolate are assumed as the ligand lengths, L_{lig}.

The optical absorption enhancement, $\mu_\lambda \,/\, \mu_\lambda^{\,0}$, ascribable to changes in the internal electric field expected upon exchanging oleate ligands for p-methylbenzenethiolate species is small, when calculated as the local field factor ratio for ligand-exchanged and as-synthesized PbS QDs, $\left|f_{LF}\right|^2 / \left|f_{LF}^{\,0}\right|^2$ (see Figure 7). The ligand-induced enhancement of QD optical absorption experimentally observed upon exchanging oleates for p-methylbenzenethiolates is instead much larger than expected by mere dielectric confinement, as reported in Figure S15 in the case of PbS QDs.

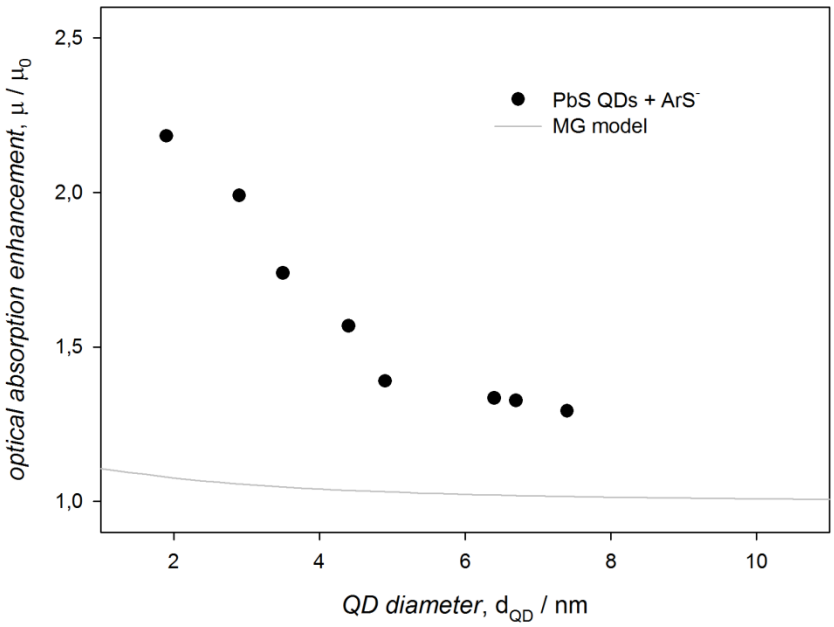

Figure S16. Experimentally determined (symbols) intrinsic absorption coefficient ratio at 400 nm of ligand-exchanged PbS QDs, μ_{400}, and as-synthesized QDs, $\mu_{400}{}^{0}$, as function of QD size, d_{QD}; dashed line represents the local field factor ratio between ligand-exchanged and as-synthesized PbS QDs as function of d_{QD}, according to equations S15-18.

Supplementary References.

S1. W. W. Yu, X. Peng, Formation of High-Quality CdS and Other II–VI Semiconductor Nanocrystals in Noncoordinating Solvents: Tunable Reactivity of Monomers. *Angew. Chem. Int. Ed.* 2002, **41**, 2368-2371.

S2. L. Carbone, C. Nobile, M. De Giorgi, F. Della Sala, G. Morello, P. Pompa, M. Hytch, E. Snoeck, A. Fiore, I. R. Franchini, I. R.; M. Nadasan, A. F. Silvestre, L. Chiodo, S. Kudera, R. Cingolani, R. Krahne, L. Manna, Synthesis and Micrometer-Scale Assembly of Colloidal CdSe/CdS Nanorods Prepared by a Seeded Growth Approach. *Nano Lett.* 2007, **7**, 2942-2950.

S3. S. Flamee, M. Cirillo, S. Abe, K. De Nolf, R. Gomes, T. Aubert, Z. Hens, Fast, High Yield, and High Solid Loading Synthesis of Metal Selenide Nanocrystals. *Chem. Mater.*, 2013, **25**, 2476–2483.

S4. M. A. Hines, G. D. Scholes, Colloidal PbS Nanocrystals with Size-Tunable Near-Infrared Emission: Observation of Post-Synthesis Self-Narrowing of the Particle Size Distribution. *Adv. Mater.* **2003**, *15*, 1844-1849.

S5. J. P. Danehy, K. N. Parameswaran, Acidic Dissociation Constants of Thiols. *J. Chem. Eng. Data* 1968, **13**, 386-389.

S6. M. Masui, H. Sayo, Y. Tsuda, Anodic Oxidation of Amines. Part I. Cyclic Voltammetry of Aliphatic Amines at a Stationary Glassy-Carbon Electrode. *J. Chem. Soc. B.* 1968, 973-976.

S7. C. Giansante, L. Carbone, C. Giannini, D. Altamura, Z. Ameer, G. Maruccio, A. Loiudice, M. R. Belviso, P. D. Cozzoli, A. Rizzo, G. Gigli, Colloidal Arenethiolate-Capped PbS Quantum Dots: Optoelectronic Properties, Self-Assembly, and Application in Solution-Cast Photovoltaics. *J. Phys. Chem. C* 2013, **117**, 13305-13317.

S8. W. W. Yu, L. Qu, W. Guo, X. Peng, Experimental Determination of the Extinction Coefficient of CdTe, CdSe, and CdS Nanorystals. *Chem. Mater.* 2003**, 15**, 2854-2860.

S9. R. K. Čapek, I. Moreels, K. Lambert, D. De Muynck, Q. Zhao, A. Van Tomme, F. Vanhaecke, Z. Hens, Optical Properties of Zincblende Cadmium Selenide Quantum Dots. *J. Phys. Chem. C*, 2010, **114**, 6371–6376.

S10. D. Debellis, G. Gigli, S. ten Brinck, I. Infante, C. Giansante, Quantum-Confined and Enhanced Optical Absorption of Colloidal PbS Quantum Dots at Wavelengths with Expected Bulk Behavior. *Nano Lett.* 2017, **17**, 1248–1254.

S11. M. T. Frederick, V. A. Amin, L. C. Cass, E. A. Weiss**,** A Molecule to Detect and Perturb the Confinement of Charge Carriers in Quantum Dots. *Nano Lett.* 2011**, 11**, 5455-5460.

S12. A. Fischer, L. Rollny, J. Pan, G. H. Carey, S. M. Thon, S. Hoogland, O. Voznyy, D. Zhitomirsky, J. Y. Kim, O. M. Bakr, E. H. Sargent, Directly Deposited Quantum Dot Solids Using a Colloidally Stable Nanoparticle Ink. *Adv. Mater.* 2013**, 25**, 5742-5749.

S13. C. Giansante, R. Mastria, G. Lerario, L. Moretti, I. Krieger, F. Scotognella, G. Lanzani, S. Carallo, M. Esposito, M. Biasiucci, A. Rizzo, G. Gigli, Molecular-Level Switching of Polymer/Nanocrystal Non-Covalent Interactions and Application in Hybrid Solar Cells. *Adv. Funct. Mater.* 2015, **25**, 111-119.

S14. C. Giansante, I. Infante, E. Fabiano, R. Grisorio, G. P. Suranna, G. Gigli, "Darker-than-Black" PbS Quantum Dots: Enhancing Optical Absorption of Colloidal Semiconductor Nanocrystals via Short Conjugated Ligands. *J. Am. Chem. Soc.* 2015, **137**, 1875-1886.

S15. D. Spirito, S. Kudera, V. Miseikis, C. Giansante, C. Coletti, R. Krahne, UV Light Detection from CdS Nanocrystal Sensitized Graphene Photodetectors at kHz Frequencies. *J. Phys. Chem. C* 2015, **119**, 23859–23864.

S16. R. Grisorio, D. Debellis, G. P. Suranna, G. Gigli, C. Giansante, The Dynamic Organic/Inorganic Interface of Colloidal PbS Quantum Dots. *Angew. Chem. Int. Ed.* 2016, **55**, 6628-6633.

S17. C. Giansante, Surface Chemistry Control of Colloidal Quantum Dot Band Gap. *J. Phys. Chem. C* 2018, **122**, 18110−18116.

S18. C. Giansante, L. Carbone, C. Giannini, D. Altamura, Z. Ameer, G. Maruccio, A. Loiudice, M. R. Belviso, P. D. Cozzoli, A. Rizzo, G. Gigli, Colloidal Arenethiolate-Capped PbS Quantum Dots: Optoelectronic Properties, Self-Assembly, and Application in Solution-Cast Photovoltaics. *Thin Solid Films* 2014, **560**, 2-9.

S19. C. A. Leatherdale, M. G. Bawendi, Observation of solvatochromism in CdSe colloidal quantum dots. *Phys. Rev. B* 2001, **63**, 165315.

S20. A. V. Rodina, Al. L. Efros, Effect of Dielectric Confinement on Optical Properties of Colloidal Nanostructures. ЖЭТФ, 2016, **149**, 641–655.

S21. J. Hunger, A. Stoppa, A. Thoman, M. Walther, R. Buchner, Broadband dielectric response of dichloromethane. *Chem. Phys. Lett.* 2009, **471**, 85-91.

S22. Y. Nosaka, Finite Depth Spherical Well Model for Excited States of Ultrasmall Semiconductor Particles. An Application. *J. Phys. Chem.* 1991, **95**, 5054-5058.

S23. D. Schooss, A. Mews, A. Eychmuller, H. Weller, Quantum dot-quantum well CdS/HgS/CdS: Theory and experiment. *Phys. Rev. B* 1994, **49**, 17072.

S24. I. Moreels, K. Lambert, D. Smeets, D. De Muynck, T Nollet, J. C. Martins, F. Vanhaecke, A. Vantomme, C. Delerue, G. Allan, Z. Hens, Size-Dependent Optical Properties of Colloidal PbS Quantum Dots. *ACS Nano* 2009, **3**, 3023-3030.

S25. A. E. Neeves, M. H. Birnboim, *J. Opt. Soc. Am. B* 1989**, 6**, 787-796.